Journal of Physics:
Condensed Matter

Anisotropic magnetoresistance in Sr_2FeMoO_6 thin films

To cite this article before publication: Akseli Nykänen Nykänen *et al* 2025 *J. Phys.: Condens. Matter* in press https://doi.org/10.1088/1361-648X/ae1c88

Anisotropic magnetoresistance in Sr_2FeMoO_6 thin films

A. Nykänen[1], I. Angervo[1], H. Huhtinen[1] and P. Paturi[1]

[1] Wihuri Physical Laboratory, Department of Physics and Astronomy, FI-20014 University of Turku, Finland

E-mail: ijange@utu.fi

27 October 2025

Abstract.

Epitaxial Sr_2FeMoO_6 films were investigated for their magnetoresistive properties. The results revealed a distinct anisotropic resistance response to the magnetic field, which was especially noticeable when the current path was oriented along different crystallographic directions. This anisotropic behavior was observed as varying symmetries in the resistance-field direction dependence. The phenomenon was discussed in the context of magnetocrystalline anisotropy as well as more general electrical properties. The findings suggest that some commonly accepted explanations for anisotropic magnetoresistance are insufficient to account for the recent observations. A deeper understanding of the electrical properties of Sr_2FeMoO_6—and similar materials—is therefore necessary. Additionally, the work demonstrated an enhancement in magnetic properties as a result of temperature annealing treatment.

1. Introduction

Multifunctional materials of high quality have garnered significant interest for future magnetoresistive and spintronic applications, where key objectives include device miniaturization, faster data transfer rates, and more precise sensors [1–3]. In this context, the ordered double-exchange perovskite Sr_2FeMoO_6 (SFMO) has emerged as a promising material due to its exceptionally high Curie temperature (T_C) exceeding 400 K and its 100% spin-polarized charge carriers [4–6]. However, fabricating SFMO thin films while maintaining its desirable electrical and magnetic properties remains challenging. This has spurred extensive efforts to optimize the preparation processes, including various annealing treatments [7–10].

Anisotropic magnetoresistance (AMR) is a phenomenon where the resistance of a material depends on the angle between the magnetic field—or saturated magnetization—and the direction of the current. In general, AMR follows the relation $\rho(\gamma) = \rho_\perp + (\rho_\parallel - \rho_\perp)\cos^2(\gamma)$, where $\rho_\parallel$ and $\rho_\perp$ represent resistivities measured when the current is parallel and perpendicular to the magnetic field, respectively [11, 12]. While this expression is valid for polycrystalline systems, AMR behavior can be more complex in single crystals, where bulk crystalline or magnetic anisotropies are not isotropic. Magnetocrystalline anisotropy is an example where the magnetization response depends on crystal orientation. Other forms of anisotropies include induced anisotropy, caused by annealing treatments; magnetoelastic anisotropy, resulting from lattice mismatch-induced strain; and surface anisotropy, where interfacial magnetic regions can break crystal symmetry [11, 13].

AMR has been widely studied in perovskite manganites, such as $La_{1-x}Ca_xMnO_3$ [14–17] and $La_{1-x}Sr_xMnO_3$ [18, 19], due to its importance in applications like magnetoresistive random access memories (MRAMs) and magnetic read heads. In ferromagnets, AMR originates from spin-orbit coupling, where the scattering rate of conduction electrons in the s band depends on the angle between the spins of localized $3d$ electrons and the current direction [12]. The linear relationship between out-of-plane anisotropy and epitaxial strain [20], as well as magnetic resonance and spin-wave relaxation studied via ferromagnetic resonance techniques [21], has been reported for SFMO films. Nevertheless, comprehensive studies of resistivity across the full angular range in both in-plane and out-of-plane directions under varying magnetic fields and temperatures remain scarce.

In this work, in addition to the optimization of post-annealing treatments and basic structural, magnetic and resistive characterizations of the SFMO thin films, we have concentrated on the angular dependent magnetoresistive properties to investigate the AMR and low field magnetoresistance (LFMR). The results are discussed in the light of magnetic configurations that are crucial when designing novel spintronic devices for future technological challenges.

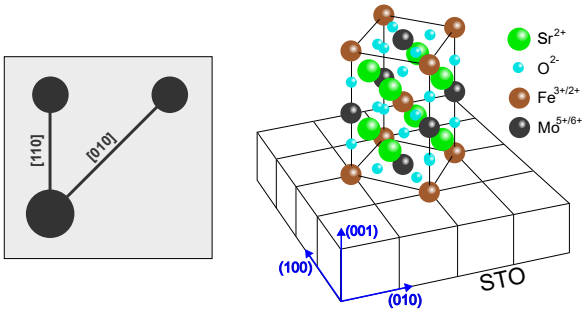

Figure 1. The schematic illustration of the patterned SFMO thin film with its crystallographic axes to show the current directions during the magnetoresistive measurements. On the right, the tetragonal SFMO unit cell is oriented so that its in-plane axes on the surface are 45° tilted from the corresponding axes of the STO (100) substrate. This means that pseudo cubic SFMO lattice is oriented according to STO in-plane axes.

2. Experimental details

The SFMO thin films with thickness of ≈120 nm were prepared by pulsed laser deposition (PLD) on $SrTiO_3$ (STO) (100) substrates using earlier optimized growth parameters such as the substrate temperature of 900°C, Ar deposition pressure of 70 mTorr and laser fluence of 1.6 J/cm^2. For the magnetoresistive measurements, the films were patterned by wet chemical etching into 100 μm wide stripes along the different crystallographic directions of [010] and [110] as schematically illustrated in Fig. 1. The length of the stripe in [110] direction is 1 mm and approximately 1.4 mm in [010] direction. Due to tetragonal symmetry of SFMO unit cell [010] is isotropic with [100]. The electrical contacts were done using TPT HB05 Wire Bonder with Al wiring. The details of the target synthesis, film deposition etc. have been published separately in [8, 10, 22].

The x-ray diffraction (XRD) studies were made at room temperature using a Panalytical Empyrean diffractometer with a 5-axes goniometer using CuK_α radiation. The crystallinity, phase purity, texture and lattice parameters were determined from $(\theta, 2\theta)$ scans in the (008) and (336) directions and from the (ϕ, ψ) texture scans accompanied by the detailed $(\phi, 2\theta)$ results of the SFMO (204) peaks. The magnetic measurements were done using a Quantum Design MPMS SQUID magnetometer with the external field parallel to the plane of the film, i.e. along the SFMO (110) direction. The temperature dependent field-cooled (FC) magnetizations were measured in 100 mT field and the Curie temperature was defined as a minimum of the temperature derivative of the FC-curve. To determine the saturation and remanence magnetizations and coercivities, the magnetic hysteresis loops were measured at 10 K and 400 K between -1000 mT and 1000 mT. The magnetoresistive properties were studied using a Quantum Design Physical Property Measurement System (PPMS) with a horizontal rotator option, applying a direction of rotation parallel and perpendicular to the film plane.

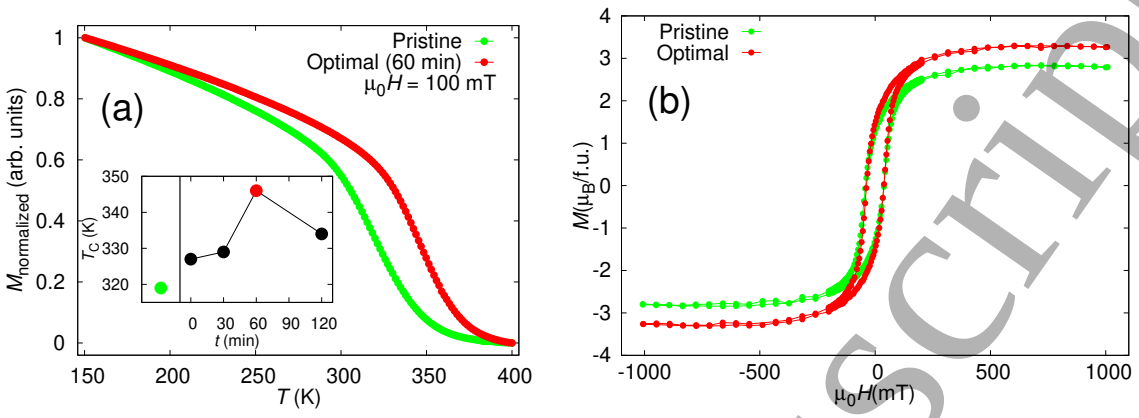

Figure 2. (a) Temperature dependence of the normalized magnetization curves of pristine untreated SFMO film and the optimally at 800°C post-annealing treated films producing improvement in T_C (the main panel). The inset shows how the annealing treatment time has an optimal value of ≈60 min. (b) Magnetization versus magnetic field hysteresis loops for the pristine film and the optimally annealed film. The results show that magnetization is saturated in 500 mT. The results are obtained for films before lithography patterning with field parallel to the plane of the film along the SFMO (110) direction.

3. Results and discussion

3.1. Optimization of structural, magnetic and magnetoresistive properties

To achieve optimal properties for the SFMO thin film, particularly maximizing the Curie temperature (T_C), we optimized the *ex situ* post-annealing treatment in a vacuum chamber with a high vacuum of 10^{-7} mbar. The annealing parameters included the temperature, ranging from room temperature up to the system's maximum of 800°C, and the annealing duration, which varied from 0 to 180 minutes. As shown in Fig. 2 (a), the highest T_C of 340 K, measured at the midpoint of the transition, with an onset T_C exceeding 400 K, was achieved by annealing the SFMO films for 60 minutes at 800°C. In comparison, the T_C of the untreated pristine film was only 319 K. The pristine sample differs from 0 min treatment in a sense that while the pristine sample has not gone through annealing treatment, in 0 min treatment the annealing temperature has been reached but the cool down begins immediately. In Fig. 2 (b) magnetization versus field hysteresis loops are presented for an optimally annealed and a pristine sample. The results show magnetization saturation around 500 mT and in higher fields. The optimally annealed sample also shows saturation magnetization above 3 μ_B / f.u., which is slightly higher compared to the pristine sample.

The crystalline quality, possible impurity phases and SFMO lattice parameters were characterized using XRD. As shown in Fig. 3 and based on the pole figures from texture scans (not shown here), the optimized films are phase-pure and exhibit topotaxial growth along the SFMO (00l) direction. From the 2D measurements (inset of Fig. 3), where the width of the (204) peak was fitted with a Gaussian function to the data measured in

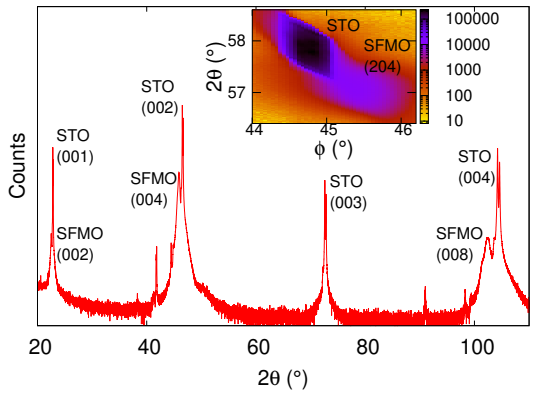

Figure 3. The room temperature x-ray 2θ diffractogram with identified SFMO film and STO substrate $(00l)$ peaks. The inset shows SFMO (204) peak intensities as a function of 2θ and ϕ, partially hided by the peak of STO substrate. The results are for optimally annealed film.

Table 1. The relevant structural properties such as SFMO lattice parameters and XRD peak widths in θ- and ϕ-directions, as well as the most important magnetic parameters of Curie temperature and saturation magnetization, remanent magnetization and the coercive field obtained from the magnetic hysteresis loops at 10 K. The results are for optimally annealed film.

Structural	a/b (Å)	c (Å)	$\Delta\theta$ (008) (°)	$\Delta\theta$ (336) (°)	$\Delta\phi$ (204) (°)
	5.568	7.912	1.493	2.601	0.778
Magnetic	$T_{C,mid}$ (K)	$T_{C,onset}$ (K)	M_s (μ_B/f.u.)	M_r (μ_B/f.u.)	$\mu_0 H_c$ (mT)
	340	400	3.27	1.47	37.5

the ϕ-direction, the SFMO peak can be identified near the STO diffraction peak, with no secondary diffraction peaks outside the expected CuK_α components. This confirms a single-phase SFMO film without significant contributions from twin boundaries.

The broadening of the SFMO (204) peak in the ϕ-direction ($\Delta\phi$), which is attributed to low-angle grain boundaries, and the broadening of the (008) and (336) peaks in the 2θ-direction ($\Delta\theta$) are consistent with our previous research results [22, 23]. The calculated lattice parameters a/b and c, as collected in Table 1, are in line with earlier grown films with similar deposition conditions as well as with the bulk values of SFMO [9, 24, 25]. The unoptimized SFMO films showed negligible differences in lattice parameter lengths and in $\Delta\phi$ compared with presented values for optimized films. However, the $\Delta\theta$ parameters for peak broadening showed slightly decreased values for optimized films. This suggests less variation in lattice parameters for optimized films.

The key magnetic results for the unpatterned and optimally annealed SFMO thin film are summarized in Table 1. The obtained $T_{C,mid}$ of 340 K, determined as the minimum of the temperature derivative of the FC curve, and the onset $T_{C,onset}$ above 400 K represent some of our highest values reported for pulsed laser-deposited SFMO thin films [22, 26, 27]. Parameters such as coercivity ($\mu_0 H_c$) and remanence

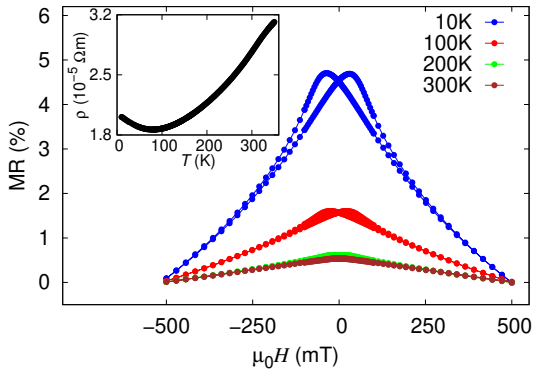

Figure 4. The magnetoresistive response for optimally annealed film measured at different temperatures, where the SFMO [110] stripe and thus the applied current are parallel to the external magnetic field (the main panel). The inset shows the temperature dependence of the resistivity measured in zero field.

magnetization (M_r) are comparable to those of previously prepared films. Notably, the saturation magnetization (M_s) is distinctly higher than in our earlier publications [9, 22, 27–29].

The basic temperature-dependent resistivity in the range of 10–350 K and the magnetoresistive (MR) responses between magnetic fields of -500 mT and 500 mT were measured at temperatures of 10 K, 100 K, 200 K, and 300 K with the SFMO [110] stripe aligned along the external magnetic field. Magnetoresistive results are presented for optimally annealed film, which has been patterned according to design in Fig. 1. The inset of Fig. 4 shows a minimum in the $\rho(T)$ curve, indicating metallic behavior with an almost linear increase above 200 K up to 350 K, and a slight upturn below 50 K, suggesting semiconducting characteristics. The semiconductive-like upturn is a common observation [24, 30–32] and we have previously proposed that the effect could be due to changes in the SFMO band gap influenced by the substrate-induced strain, oxygen vacancies, or anti-site disorder between transposed Fe and Mo atoms in the lattice [24, 32].

The MR curves, calculated using $MR = (R_B - R_{500mT})/R_{500mT}$, where R_B is the resistance at field B and R_{500mT} is the resistance at 500 mT, are presented in the main panel of Fig. 4. The results show that MR is inversely proportional to temperature, consistent with a weakening of spin-polarized electron transfer through the junction interface resulting in diminished magnetoresistance signal [33]. The low-field magnetoresistance (LFMR), associated with spin-polarized tunneling between ferrimagnetic grains separated by grain boundaries [24, 34], exhibits a hysteretic maximum slightly shifted from zero field. The maxima, such as the LFMR response of 4.7% at 10 K and 1.5% at 100 K in fields of 34 mT and 25 mT, respectively, are close to previously reported coercivity values, differing by only 12%. This correlation aligns with the influence of structural defects [35].

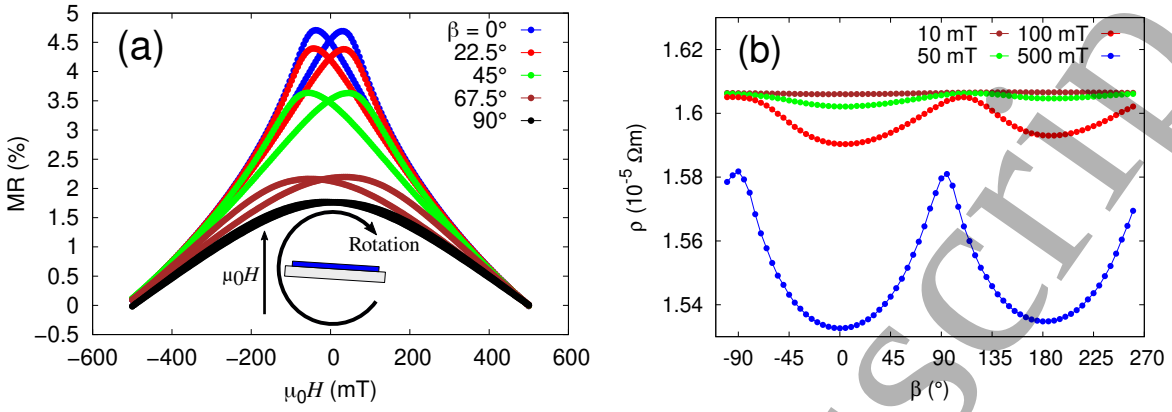

Figure 5. (a) The magnetoresistive response measured in different angles at $T = 10\,\mathrm{K}$, where the inset shows the angular configurations between the magnetic field and the film. The magnetic field points always upwards and the current is along the SFMO [110] direction, whereas at $\beta = 0°$ and 180° the current vector and the magnetic field are parallel and at 90° and 270° perpendicular to each other. (b) The angle β dependent resistivity measured at different magnetic fields of 10, 50, 100 and 500 mT.

3.2. Angular dependent magnetoresistive properties

3.2.1. Out-of-plane measurements

Similar magnetic field-dependent MR responses for optimally annealed and accordingly patterned samples were measured for both the SFMO [110] and [010] stripes at 10 K by varying the angle between the current and the field, as schematically illustrated in the inset of Fig. 5(a). In this setup, the rotational axis is perpendicular to the film's normal vector. The rotation angle β at 0° corresponds to the alignment where the film plane is parallel to the magnetic field vector. β refers to the angle between SFMO stripe i.e current and magnetic field.

As shown for the [110] stripe in Fig. 5(a), the low-field MR is roughly tripled when the film plane is parallel to the field. The results for the [010] stripe were practically identical. This phenomenon partly reflects the demagnetizing effect of the film's shape, meaning that a larger field is required to compensate for the demagnetizing effect when the LFMR is measured with the field applied parallel or close to the surface normal vector ($\beta = 90°$ and $\beta = 67.5°$ scans). This results in an apparent shift and broadening of the magnetic field corresponding to the hysteretic resistance maxima in LFMR, as demonstrated in previous reports [36–38]. Additional AMR and pinning effects may also contribute to the observed behavior, but a rigorous analysis of their contributions in this case is not practical.

Based on the rotationally symmetric resistivity measurements under different external magnetic fields (Fig. 5(b)), one can easily observe a magnetic two-fold symmetry, with maxima in resistivity occurring when the normal vector of the sample surface is parallel to the field. The angular dependence of ρ in a constant magnetic field

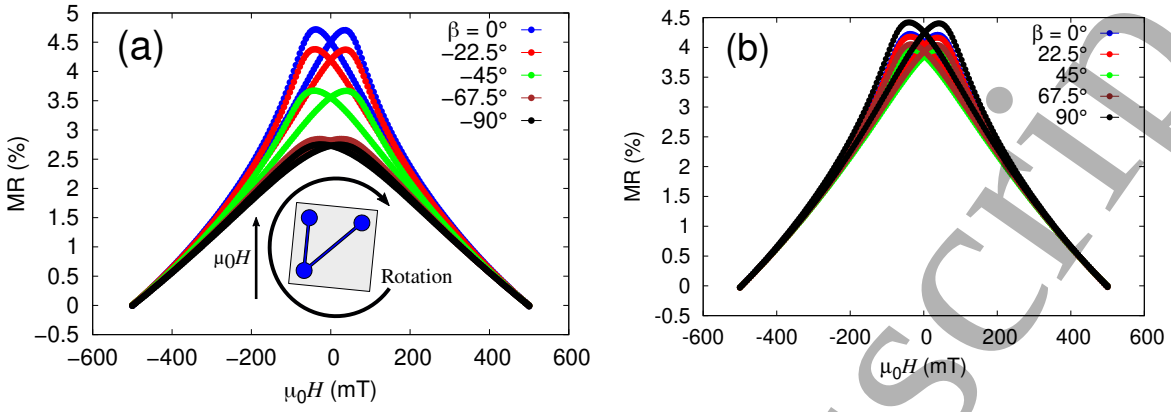

Figure 6. The magnetoresistive response measured at 10 K in different angles between magnetic field and current, with two different applied current configurations, along the SFMO [110] direction (a) and [010] direction (b). As shown in the inset of (a), the magnetic field points always upwards. The angle of 0° in (a) corresponds the current vector parallel to the direction of magnetic field and 90° (-90°) corresponds to perpendicular direction.

illustrates the regular AMR response, where $\rho \propto \cos^2(\gamma)$, and γ refers to the angle between the current and the magnetization. The slight deviation of the resistance maxima from $\beta = 90°$ in the 100 mT scan could be attributed to shape-induced anisotropy and/or coercivity. This is because the demagnetizing effects are more significant when the magnetic field is perpendicular to the film plane, and the field is still below the strength needed to fully saturate the magnetization, which may also apply to 500 mT results. However, the results obtained in 500 mT with magnetic field parallel with film plane are for magnetization in saturation. This is confirmed by the magnetization versus field hysteresis results presented in Fig. 2 (b).

3.2.2. In-plane measurements

Magnetoresistance measurements were also conducted by rotating the sample in a full in-plane orientation, where the normal vector of the sample remains perpendicular to the external magnetic field throughout the entire angular range. The correspondence between the magnetic field direction and the alignment of the sample stripe, i.e., the current direction, is schematically illustrated in the inset of Fig. 6(a).

When examining the magnetic field dependencies of LFMR at different angles between the current and the field in Figs. 6(a) and (b), a clear distinction between the [110] and [010] SFMO stripes is observed. The variation of LFMR in the [010] direction is negligible, whereas in the [110] stripe, the LFMR is significantly higher when the current is parallel to the magnetic field ($\beta = 0°$ scan). The shape-induced demagnetization or differences in Lorentz force-induced magnetoresistance cannot explain the observed discrepancies between the results for the [110] and [010] stripes in Figs. 6(a) and (b).

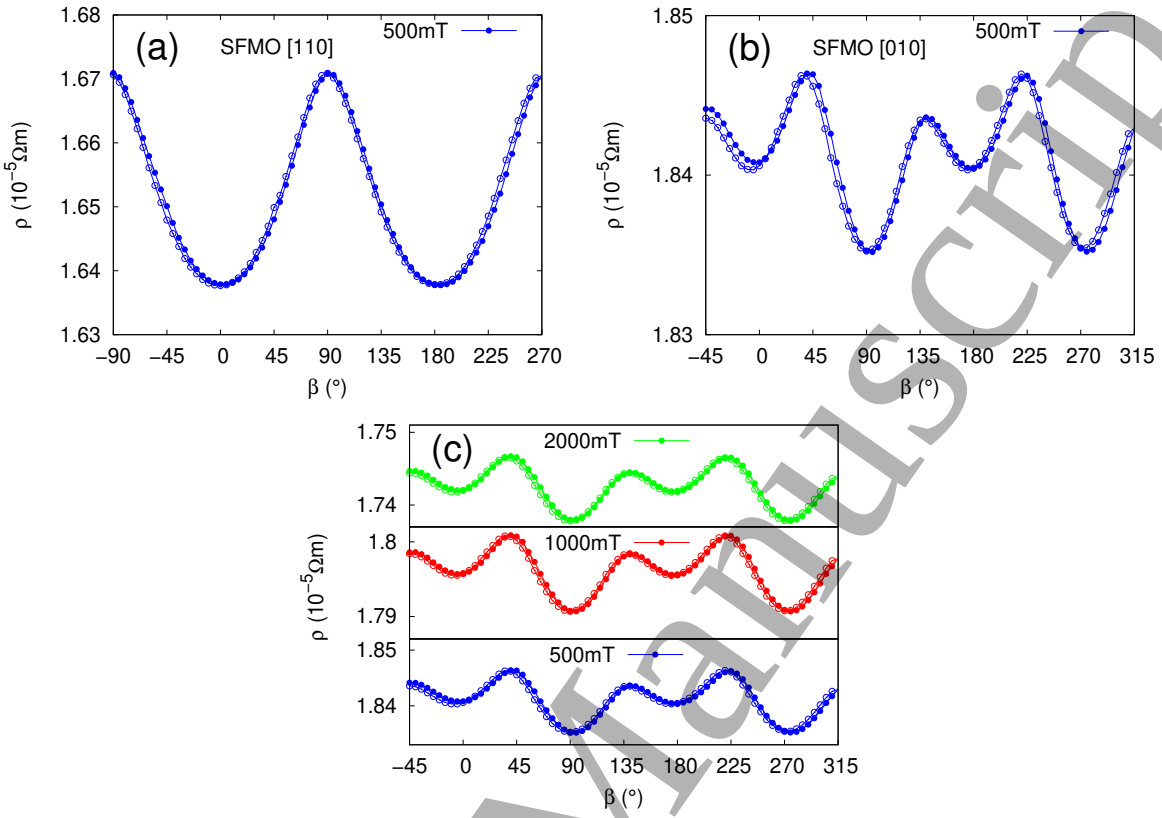

Figure 7. The rotation angle dependence of resistivity measured in the magnetic field of 500 mT with the current vector along the SFMO [110] (a) and [010] direction (b). The angle between the directions of current and magnetic field is as explained in the figure caption of Fig. 6. In (c) the respective high field results are presented as in (b) for SFMO [010] direction. All the results are presented for clockwise and counterclockwise rotation.

This is because the LFMR data were obtained under symmetrical field vs. current configurations, and the differences in demagnetization effects due to variations in stripe length are negligible.

The phenomenon of LFMR with varying magnetic field—or magnetization—orientation relative to the current, crystalline axes, and magnetic easy axes has been studied in comparable materials [39–44]. A hysteretic LFMR phenomenon, due to spin transport between magnetically oriented domains, is accompanied by AMR when the angular orientation between the current and magnetization is varied. Notably, the absolute resistance in the $\beta = 90°$ LFMR scan is higher than in other orientations, which are shown in Fig. 6(a). This indicates that the AMR effect weakens the resistivity drop in LFMR, which is due to spin-dependent transport of charge carriers and the reorientation of magnetic moments. This reasoning aligns with the multidomain model presented by O'Donnell et al. [39]. Similar results, where the magnetic field orientation relative to the current affects LFMR, are commonly observed, though the studies often emphasize different aspects [39–44]. In Fig. 6(b), the LFMR is less influenced by β

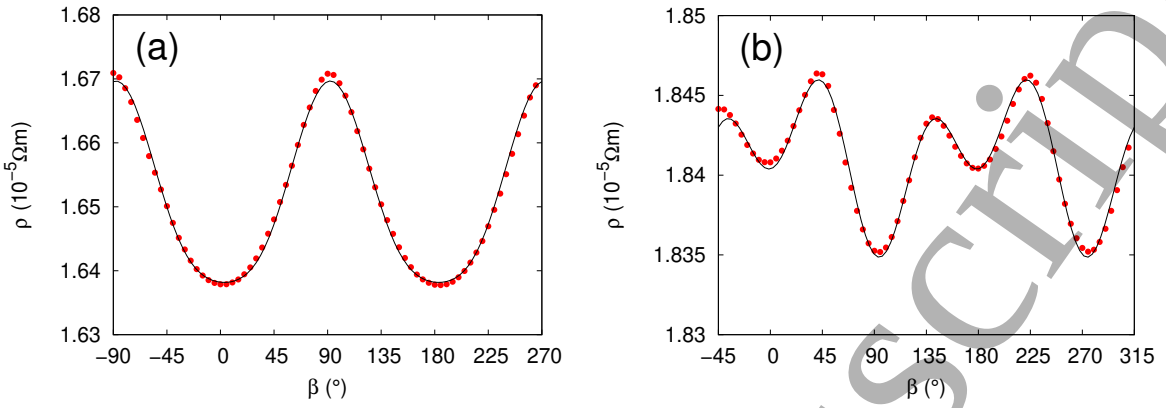

Figure 8. The resistance plotted as a function of the angle between the magnetic field direction and the in-plane rotating current, which is applied along the SFMO [110] (a) and [010] direction (b), respectively. The fit to the data is done using the phenomenological model given in Eq. 1 [16].

compared to Fig. 6(a), demonstrating the difference in AMR between the two SFMO stripes prepared along different crystallographic directions.

These findings are further illustrated in Figs. 7(a), (b) and (c). The results in (a) and (b) are presented for 500 mT measurements, where SFMO film is in saturation. Additional high field results measured in 1000 mT and 2000 mT are presented in (c) and the results showed no distinction in angle dependence confirming the saturation of magnetization. The results again confirm that the longitudinal resistivity depends strongly on the orientation of the magnetic moment and the current direction relative to the crystallographic axes. As observed in the out-of-plane measurements, a two-fold symmetry with a 180° period is evident in the [110] stripe. The maxima in ρ occur when the current is perpendicular to the magnetic field, and as in the out-of-plane case, this behavior illustrates the regular $\rho \propto \cos^2(\gamma)$ response of anisotropic magnetoresistance.

For the [010] stripe, similar measurements in a 500 mT field reveal a 180° period, where minima occur when the current is perpendicular to the magnetic field. However, additional local minima are observed when the current is parallel to the field, resulting in a clear four-fold symmetry in ρ for the SFMO [010] direction. This four-fold symmetry cannot be explained by regular AMR or Lorentz force effects, and the mechanism underlying this particular anisotropy is thoroughly discussed in the following section.

3.3. Phenomenological model and mechanism

The regular AMR dependence, where $\rho \propto \cos^2(\gamma)$, does not account for the anisotropic effects of crystal symmetry. Indeed, deviations from this behavior, reflecting higher-order symmetry, have been demonstrated in various epitaxial crystal systems [16, 19, 39, 45–47]. In our in-plane magnetoresistance measurements, two clearly distinct symmetry components were observed, depending on the transport current direction along the SFMO crystallographic axes. To understand the mechanism, we attempted to fit the

Table 2. The fitting parameters when the angular dependent resistance data measured in 500 mT field and in both SFMO [110] and [010] directions is fitted to the phenomenological model given in Eq. 1.

Stripe	$C_0''(\Omega)$	$C_1''(\Omega)$	$C_2''(\Omega)$
[110]	2.06	-0.02	0.003
[010]	3.25	0.005	-0.006

angular-dependent resistance using a phenomenological model [16].

This model was originally applied to the $La_{2/3}Ca_{1/3}MnO_3$ (LCMO) perovskite with tetragonal symmetry, accounting for the same in-plane rotation of magnetization. The magnetization is always aligned perpendicular to the $(00l)$ direction, meaning it is perpendicular to the film normal vector, as in our experimental setting. In [16], the longitudinal resistance is expressed as:

$$R_{\mathrm{xx}} = C_0'' + C_1'' \cos 2\phi_{\mathrm{M}} + C_2'' \cos 4\phi_{\mathrm{M}} + C_{\mathrm{m}} \sin 2\phi_{\mathrm{M}}, \tag{1}$$

where ϕ_{M} is the angle between the magnetic field and the in-plane rotating current. This is connected to a biaxial anisotropy related to the lattice in-plane square symmetry, along with two-fold and four-fold uniaxial anisotropies of the current. The fitting parameters C_0'', C_1'', C_2'', and C_{m} correspond to the symmetrical and antisymmetrical parts of the dynamic transport property tensor. Here, C_0'' represents the baseline resistance, while C_{m} accounts for slight misalignment, which is relatively small compared to C_1'' and C_2''. A good agreement between the fit and the data for both the [110] and [010] directions, measured in a 500 mT field, is shown in Fig. 8, along with the obtained fitting parameters in Table 2.

Although extending the resistivity tensor is a reasonable approach, this phenomenological reasoning does not necessarily provide a direct link to the underlying origins of the phenomenon. One proposed origin of the four-fold symmetry observed in longitudinal resistivity measurements is magnetocrystalline anisotropy [45, 48–51]. Magnetocrystalline anisotropy arises in part due to crystal symmetry, and an identical symmetry is expected between the crystal structure and the magnetization field response. This symmetry gives rise to easy- and hard-magnetization axes, which are alleged to contribute to resistance. While magnetocrystalline anisotropy contributes a symmetrical component to the energy required to align magnetic moments parallel to the field, attributing the additional symmetry in our $\rho(\beta)$ data solely to magnetocrystalline anisotropy seems overly simplistic. Our data already demonstrates that the AMR effect depends on the choice of current direction, whereas magnetocrystalline anisotropy should remain practically identical. Consequently, the four-fold symmetry term shown in Table 2 should also be equal between the two current directions. Furthermore, the saturated SFMO system shows no signs of losing the four-fold symmetry in $\rho(\beta)$ at high fields, where the relative contribution of magnetocrystalline anisotropy to the free energy should be decreasing.

In the case of manganites, the anisotropic conduction properties could be influenced by orbital deformation induced by magnetization alignment, which affects the double-exchange hopping conduction. This, in turn, could explain the AMR and the two distinct symmetry phenomena observed along the SFMO crystallographic axes [110] and [010], as the angle between the magnetic field and the current changes, as discussed by O'Donnell et al. [39]. A more detailed understanding of anisotropic magnetoresistance in other materials has been obtained by demonstrating competitive magnetization effects on the band structure, where band gaps with opposite angular dependence on magnetization rotation influence conduction [52]. This effect also depends on the alignment of the current relative to the crystal axes. According to electron scattering theory, four-fold symmetry can arise from orbital hybridization, which depends on the partial density of states at the Fermi level [53]. The relevance of band structure symmetry to AMR has also been highlighted [54]. The interface induced effects can potentially also induce four-fold symmetry in AMR [55], but we consider this as unlikely cause in our results.

Considering these observations, it is possible that the four-fold symmetry in our ρ results is influenced by magnetocrystalline anisotropy, which partially originates from spin-orbit coupling. However, in a more general sense, the anisotropic nature of the electronic structure in our SFMO films likely provides the foundation for anisotropic magnetoresistance. Spin-orbit coupling also influences the electronic band structure, but it remains unclear whether magnetocrystalline anisotropy, often cited as the source of four-fold AMR symmetry, is the definitive cause of the phenomenon. SFMO, as a half-metallic material with a spin-polarized band at the Fermi level, is driven by the hybridization of Mo and Fe d-states through oxygen [4, 5, 56, 57]. This intrinsic property strongly suggests the anisotropic nature of transport properties in epitaxial systems. Moreover, the electronic structure of SFMO is known to be influenced by anti-site disorder, which has been shown to enhance the four-fold resistance response in other materials through band structure modifications [58]. Although the anisotropic nature of magnetic or electric properties has not yet been thoroughly demonstrated or established for SFMO, intrinsic mechanisms observed in other materials provide insight into potential explanations for this phenomenon.

4. Conclusions

We have demonstrated an enhancement of Curie temperature in epitaxial SFMO thin films, obtained through optimized temperature annealing treatment. The optimized films have been studied for their magnetoresistive properties. The research revealed that the properties are strongly anisotropic. Magnetoresistance is influenced by demagnetization effects but this alone cannot explain the results. Indeed the four fold symmetry in anisotropic magnetoresistance is therefore an indication of intrinsic anisotropic electrical structure, but could be also linked to magnetocrysalline anisotropy.

Acknowledgements

Jenny & Antti Wihuri Foundation is acknowledged for financial support.

References

[1] Baibich M N, Broto J M, Fert A, Dau F N V, Petroff F, Eitenne P, Creuzet G, Friederich A and Chazelas J 1988 Giant magnetoresistance of (001)Fe/(001)Cr magnetic superlattices *Phys. Rev. Lett.* **61** 2472

[2] Wolf S A, Awschalom D D, Buhrman R A, Daughton J M, von Molnár S, Roukes M L, Chtchelkanova A Y and Treger D M 2001 Spintronics: A spin-based electronics vision for the future *Science* **294** 1488

[3] Tokura Y and Hwang H Y 2008 Complex oxides on fire *Nature Mater.* **7** 694

[4] Kobayashi K I, Kimura T, Sawada H, Terakura K and Tokura Y 1998 Room-temperature magnetoresistance in an oxide material with an ordered double-perovskite structure *Nature* **395** 677

[5] Tomioka Y, Okuda T, Okimoto Y, Kumai R, Kobayashi K I and Tokura Y 2000 Magnetic and electronic properties of a single crystal of ordered double perovskite Sr_2FeMoO_6 *Phys. Rev. B* **61** 422

[6] Bibes M, Bouzehouane K, Barthelemy A, Besse M, Fusil S, Bowen M, Seneor P, Carrey J, Cros V, Vaures A, Contour J P and Fert A 2003 Tunnel magnetoresistance in nanojunctions based on Sr_2FeMoO_6 *Appl. Phys. Lett.* **83** 2629

[7] Sanchez D, Auth N, Jakob G, Martinez J L and Garcia-Hernandes M 2005 Pulsed laser deposition of Sr_2FeMoO_6 thin films *J. Magn. and Magn. Mater.* **294** e119

[8] Paturi P, Metsänoja M and Huhtinen H 2011 Optimization of deposition temperature and atmosphere for pulsed laser deposited Sr_2FeMoO_6 thin films *Thin Solid Films* **519** 8047

[9] Saloaro M, Hoffmann M, Adeagbo W A, Granroth S, Deniz H, Palonen H, Huhtinen H, Majumdar S, Laukkanen P, Hergert W, Ernst A and Paturi P 2016 Toward versatile Sr_2FeMoO_6-based spintronics by exploiting nanoscale defects *ACS Appl. Mater. Interfaces* **8** 20440

[10] Saloaro M, Liedke M O, Angervo I, Butterling M, Hirschmann E, Wagner A, Huhtinen H and Paturi P 2021 Exploring the anti-site disorder and oxygen vacancies in Sr_2FeMoO_6 thin films *J. Magn. and Magn. Mater.* **540** 168454:1–6

[11] Coey J M D 2010 *Magnetism and Magnetic Materials* (Cambridge University Press)

[12] Mcguire T R and Potter R I 1975 Anisotropic Magnetoresistance in Ferromagnetic 3d Alloys *IEEE Transactions on Magnetics* **11** 1018

[13] Getzlaff M 2008 *Fundamentals of Magnetism* (Springer)

[14] Eckstein J N, Bozovic I, O'Donnell J, Onellion M and Rzchowski M S 1996 Anisotropic magnetoresistance in tetragonal $La_{1-x}Ca_xMnO_\delta$ thin films *Appl. Phys. Lett.* **69** 1312–1314

[15] O'Donnell J, Eckstein J N and Rzchowski M S 2000 Temperature and magnetic field dependent transport anisotropies in $La_{0.7}Ca_{0.3}MnO_3$ films *Appl. Phys. Lett.* **76** 218–220

[16] Li J, Li S L, Wu Z W, Li S, Chu H F, Wang J, Zhang Y, Tian H Y and Zheng D N 2010 A phenomenological approach to the anisotropic magnetoresistance and planar hall effect in tetragonal $La_{2/3}Ca_{1/3}MnO_3$ thin films *J. Phys. Cond. Mat.* **22** 146006:1–9

[17] Egilmez M, Chow K H and Jung J A 2011 Anisotropic magnetoresistance in perovskite manganites *Mod. Phys. Lett. B* **25** 697–722

[18] Yau J B, Hong X, Posadas A, Ahn C H, Gao W, Altman E, Bason Y, Klein L, Sidorov M and Krivokapic Z 2007 Anisotropic magnetoresistance in colossal magnetoresistive $La_{1-x}Sr_xMnO_3$ thin films *J. Appl. Phys.* **102** 103901:1–6

[19] Bason Y, Hoffman J, Ahn C H and Klein L 2009 Magnetoresistance tensor of $La_{0.8}Sr_{0.2}MnO_3$ *Phys. Rev. B* **79** 092406

[20] Du C, Adur R, Wang H, Hauser A J, Ysang F and Hammel P C 2013 Control of magnetocrystalline

anisotropy by epitaxial strain in double perovskite Sr_2FeMoO_6 films *Phys. Rev. Lett.* **110** 147204:1–5

[21] Nosach T, Mullady G, Leifer N, Adyam V, Li Q, Greenbaum S and Ren Y 2008 Angular dependence of spin-wave resonance and relaxation in half-metallic $Sr_2FeMo\ O_6$ films *J. Appl. Phys.* **103** 07E311:1–3

[22] Angervo I, Saloaro M, Tikkanen J, Huhtinen H and Paturi P 2017 Improving the surface structure of high quality Sr_2FeMoO_6 thin films for multilayer structures. *Appl. Surf. Sci.* **396** 754

[23] Angervo I, Saloaro M, , Huhtinen H and Paturi P 2017 Interface defects induced vertical magnetic anisotropy in Sr_2FeMoO_6 thin films. *Appl. Surf. Sci.* **422** 682

[24] Saloaro M, Majumdar S, Huhtinen H and Paturi P 2012 Absence of traditional magnetoresistivity mechanisms in Sr_2FeMoO_6 thin films grown on $SrTiO_3$, MgO and $NdGaO_3$ substrates *J. Phys. Cond. Mat.* **24** 366003

[25] Saloaro M, Deniz H, Huhtinen H, Palonen H, Majumdar S and Paturi P 2015 The predominance of substrate induced defects in magnetic properties of Sr_2FeMoO_6 thin films *J. Phys. Cond. Mat.* **27** 386001:1–11

[26] Saloaro M 2015 *The role of structural imperfections in Sr_2FeMoO_6 thin films* (väitöskirja, Turun yliopisto)

[27] Angervo I, Saloaro M, Palonen H, Majumdar S, Huhtinen H and Paturi P 2015 Thickness dependent properties of Sr_2FeMoO_6 thin films grown on $SrTiO_3$ and $(LaAlO_3)_{0.3}(Sr_2AlTaO_6)_{0.7}$ substrates *20th International Conference on Magnetism* **75** 1011

[28] Angervo I, Saloaro M, Mäkelä J, Lehtiö J P, Huhtinen H and Paturi P 2018 Surface topography and electrical properties in Sr_2FeMoO_6 films studied at cryogenic temperatures *J. Phys.: Conf. Ser.* **969** 012107

[29] Angervo I, Saloaro M, Granroth S, Huhtinen H and Paturi P 2020 Refined Sr_2FeMoO_6 interface realized with photoemission and magnetization analysis *Appl. Surf. Sci.* **507** 144435

[30] Manako T, Izumi M, Konishi Y, Kobayashi K I, Kawasaki M and Tokura Y 1999 Epitaxial thin films of ordered double perovskite Sr_2FeMoO_6 *Appl. Phys. Lett.* **74** 2215

[31] Venimadhav A, Sher F, Attfield J P and Blamire M G 2004 Oxygen assisted deposition of Sr_2FeMoO_6 thin films on $SrTiO_3(100)$ *J. Magn. and Magn. Mater.* **269** 101

[32] Saloaro M, Majumdar S, Huhtinen H and Paturi P 2013 The effect of film thickness on the magnetic and magneto-transport properties of Sr_2FeMoO_6 thin films *EPJ Web of Conferences* **40** 15012

[33] Hagler T, Kinder R and Bayreuther G 2001 Temperature dependence of tunnel magnetoresistance *J. Appl. Phys.* **89** 7570

[34] Majumdar S, Huhtinen H, Majumdar H and Paturi P 2012 Stress and defect induced enhanced low field magnetoresistance and dielectric constant in $La_{0.7}Sr_{0.3}MnO_3$ thin films *J. Alloys Compd.* **512** 332

[35] Jiles D and Atherton D 1986 Theory of ferromagnetic hysteresis *J. Magn. Magn. Mater.* **61** 48

[36] Stankevic V, Zurauskiene N, Kersulis S, Plausinaitiene V, Lukose R, Klimantavicius J, Tolvaišienė S, Skapas M and Balevicius A S S 2022 Nanostructured Manganite Films Grown by Pulsed Injection MOCVD: Tuning Low- and High-Field Magnetoresistive Properties for Sensors Applications *Sensors* **22** 605

[37] Sinha U K, Sahoo A and Padhan P 2023 Enhanced low-field positive magnetoresistance and magnetic anisotropy in $La_{0.7}Sr_{0.3}MnO_3$ films grown on (001) Si *J. Alloys Compd.* **952** 170037

[38] Srivastava M K, Singh M P, Kaur A, Razavi F S and Singh H K 2011 Low field anisotropic colossal magnetoresistance in $Sm_{0.53}Sr_{0.47}MnO_3$ thin films *J. Appl. Phys.* **110** 123922

[39] O'Donnell J, Onellion M, Rzchowski M S, Eckstein J N and Bozovic I 1997 Low-field magnetoresistance in tetragonal $La_{1-x}Ca_xMnO_3$ films *Phys. Rev. B* **55** 5873

[40] Xu Y, Dworak V, Drechsler A and Hartmann U 1999 Anisotropic low-field magnetoresistance of polycrystalline manganite sensors *Appl. Phys. Lett.* **74** 2513

[41] Li X W, Gupta A, Xiao G and Gong G Q 1997 Low-field magnetoresistive properties of polycrystalline and epitaxial perovskite manganite films *Appl. Phys. Lett.* **71** 1124

[42] Mandal S 2011 A Comparative Study of Angle Dependent Magnetoresistance in [001] and [110] $La_{2/3}Sr_{1/3}MnO_3$ *J. Supercond. Nov. Magn.* **24** 1501

[43] Amaral V, Lourenço A, ArauHjo J, Tavares P, Alves E, Sousa J, Vieira J, da Silva M and Soares J 2000 Anisotropic transport properties of epitaxial $La_{2/3}Ca_{1/3}MnO_3$ thin films with different growth orientations *J. Magn. and Magn. Mater.* **211** 1

[44] Grigaliūnaitė-Vonsevičienė G and Vengalis B 2022 Angle-dependent AC susceptibility, low-field magnetoresistance and switching behaviour of $La_{0.66}Sr_{0.34}MnO_3$/YSZ(001) films *J. Magn. and Magn. Mater.* **552** 169197

[45] Bibes M, Martinez B, Fontcuberta J, Trtik V, Ferrater C, Sanchez F, Varela M, Hiergeist R and Steenbeck K 2000 Anisotropic magnetoresistance of (00h), (0hh) and (hhh) $La_{2/3}Sr_{1/3}MnO_3$ thin films on (001) Si substrates *J. Magn. and Magn. Mater.* **211** 206

[46] Rout P K, Agireen I, Maniv E, Goldstein M and Dagan Y 2017 Six-fold crystalline anisotropic magnetoresistance in the (111) $LaAlO_3/SrTiO_3$ oxide interface *Phys. Rev. B* **95** 241107

[47] Naftalis N, Kaplan A, Schultz M, Vaz C A F, Moyer J A, Ahn C H and Klein L 2011 Field-dependent anisotropic magnetoresistance and planar Hall effect in epitaxial magnetite thin films *Phys. Rev. B* **84** 094441

[48] Gong J, Zheng D, Li D, Jin C and Bai H 2018 Lattice distortion modified anisotropic magnetoresistance in epitaxial $La_{0.67}Sr_{0.33}MnO_3$ thin films *J. Alloys Compd.* **735** 1152

[49] Li P, Jin C, Jiang E Y and Bai H L 2010 Origin of the twofold and fourfold symmetric anisotropic magnetoresistance in epitaxial Fe_3O_4 films *J. Appl. Phys.* **108** 093921

[50] Burema A A and Banerjee T 2021 Temperature-dependent periodicity halving of the in-plane angular magnetoresistance in $La_{0.67}Sr_{0.33}MnO_3$ thin films on $LaAlO_3$ *Appl. Phys. Lett.* **119** 011901

[51] Li R, Jin C and Haili B 2024 Sign reversal and symmetry change of anisotropic magnetoresistance in antiferromagnetic LSMO films *J. Appl. Phys.* **136** 043901

[52] Zeng F L, Ren Z Y, Li Y, Zeng J Y, Jia M W, Miao J, Hoffmann A, Zhang W, Wu Y Z and Yuan Z 2020 Intrinsic mechanism for anisotropic magnetoresistance and experimental confirmation in Co_xFe1-x single-crystal films *Phys. Rev. Lett.* **125** 097201

[53] Kokado S and Tsunoda M 2015 Twofold and fourfold symmetric anisotropic magnetoresistance effect in a model with crystal field *Jpn. J. Appl. Phys.* **84** 094710

[54] Zhang S, Wu Q, Liu Y and Yazyev O V 2019 Magnetoresistance from fermi surface topology *Phys. Rev. B* **99** 035142

[55] Yadav S, Gupta S K, Verma M, Paul D, Rashid A, Chalke B, Bapat R, Kulkarni N, Gautam A, Kashyap A and Chatterjee S 2025 Fourfold anisotropic magnetoresistance in antiferromagnetic epitaxial thin films of $MnPt_xPd_{1-x}$ *Phys. Rev. B* **112** 014410

[56] Sarma D D, Mahadevan P, Saha-Dasgupta T, Ray S and Kumar A 2000 Electronic structure of Sr_2FeMoO_6 *Phys. Rev. Lett.* **85** 2549

[57] Samanta S, Mishra S B, and Nanda B R K 2018 Quantum well structure of a double perovskite superlattice and formation of a spin-polarized two-dimensional electron gas *Phys. Rev. B* **98** 115155

[58] Zhang M, Peng B, Zhang W and Zhang W 2023 Effect of atomic anti-site disorder on the anisotropic magnetoresistance in Fe50Co50 alloys *Journal of Physics: Condensed Matter* **35** 395803